Laser-Ion Lens and Accelerator

Tianhong Wang,[1] Vladimir Khudik,[1,2] and Gennady Shvets[1]
[1]School of Applied and Engineering Physics, Cornell University, Ithaca, New York 14850, USA
[2]Department of Physics and Institute for Fusion Studies, The University of Texas at Austin, Austin, Texas 78712, USA

(Received 28 April 2020; revised 31 October 2020; accepted 23 December 2020; published 14 January 2021)

Generation of highly collimated monoenergetic relativistic ion beams is one of the most challenging and promising areas in ultraintense laser-matter interactions because of the numerous scientific and technological applications that require such beams. We address this challenge by introducing the concept of laser-ion lensing and acceleration. Using a simple analogy with a gradient-index lens, we demonstrate that simultaneous focusing and acceleration of ions is accomplished by illuminating a shaped solid-density target by an intense laser pulse at $\sim 10^{22}$ W/cm^2 intensity, and using the radiation pressure of the laser to deform or focus the target into a cubic micron spot. We show that the laser-ion lensing and acceleration process can be approximated using a simple deformable mirror model and then validate it using three-dimensional particle-in-cell simulations of a two-species plasma target composed of electrons and ions. Extensive scans of the laser and target parameters identify the stable propagation regime where the Rayleigh-Taylor-like instability is suppressed. Stable focusing is found at different laser powers (from a few to multiple petawatts). Focused ion beams with the focused density of order 10^{23} cm^{-3}, energies in access of 750 MeV, and energy density up to 2×10^{13} J/cm^3 at the focal point are predicted for future multipetawatt laser systems.

DOI: 10.1103/PhysRevLett.126.024801

Introduction and motivation.—A focusing optical lens is one of the oldest and best-known scientific instruments. The operating principle of a lens can be understood through either a wave or corpuscular description: by causing a photon impinging on its central portion to travel a longer distance inside the lens than a photon impinging on its periphery, we can ensure that both photons reach the focal point at the same time. Thus, focusing is ensured by the judicious variation of the lens thickness: thicker at the center, thinner at the edge. Motivated by the working principle of an optical lens focusing light using shaped matter, we pose the following question: is it possible to focus matter using light?

The key to developing such a "matter lens" is the realization that, just as matter can change the velocity and direction of a photon, an intense flux of photons can do the same for the matter. This can be accomplished using the concept of radiation pressure acceleration (RPA) [1–5] developed in the context of laser-ion acceleration of thin targets. The idea is schematically illustrated in Fig. 1, where the target is shaped in such a way that its outer (thinner) regions are accelerated to higher velocities than its central (thicker) region. We analytically demonstrate that, for a judicious choice of target thickness distribution, the resulting continuous velocity variation across the target enables its focusing into an infinitesimal spot. The important feature of RPA-based focusing of matter is that the target is focused *and* accelerated. Hence, we refer to this scheme as laser-ion lensing and acceleration (LILA).

Just as the wave nature of light prevents its focusing to a geometric point by an optical lens, several fundamental plasma effects impose limits on the minimal focal spot of a realistic laser-propelled target. Those effects include Coulomb explosions [6] and a Rayleigh-Taylor (RT)-like instability [3,7–9], which are known to break up constant-thickness targets, as well as plasma heating by the laser pulse [10–12]. Under a simplifying assumption about the target as an initially cold two-species (electrons and protons) plasma, we describe the results of our particle-in-cell (PIC) simulations and demonstrate that the RT-like instability and Coulomb explosions are effectively

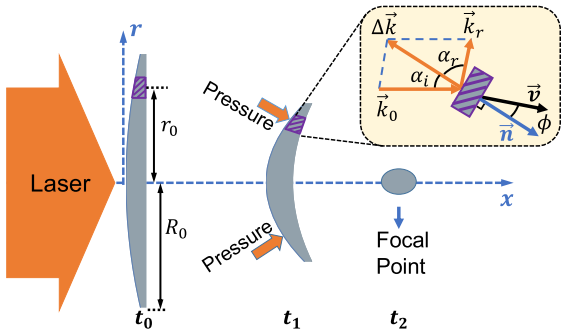

FIG. 1. Schematic of the LILA concept: a laser beam propels a thin dense target with nonuniform thickness. Inset: the geometry of the laser reflection from a small target element moving with velocity $\vec{v}$.

suppressed in a converging flow of the plasma. The result of the LILA mechanism is a quasimonoenergetic and nearly neutral relativistic beam that is both tightly focused and (due to its ultralow emittance) weakly divergent. The scientific and industrial applications of such beams are wide ranging, e.g., fast ignition of fusion targets [13,14], production of warm dense matter [15,16], hadron cancer therapy [17–19], and particle nuclear physics [20,21].

The LILA concept owes its feasibility to recent advances in laser technology that have enabled the generation of ultrashort pulses with intensities well above $I_{\mathrm{rel}} = 1.37 \times 10^{18}$ W/cm^{-2} [22] corresponding to the normalized vector potential $a_0 \equiv eA/m_e c \sim 1$ for the laser wavelength $\lambda_0 \equiv 2\pi c/\omega_0 = 1$ μm, where A is the laser vector potential, c is the speed of light, $-e$ and m_e are the electron charge and mass, and ω_0 is the laser frequency. In addition to the RPA regime, where an overdense thin target is propelled by the radiation pressure $P = 2I/c$ of a circular polarized laser with ultrahigh intensity $I > 10^{21}$ W/cm^2 [9,23,24], several compelling ion accelerating scenarios are currently under investigation. Those include target normal sheath acceleration (TNSA) [25,26] and shock wave [27,28] and laser breakout afterburner [29] acceleration.

In the TNSA regime, ion focusing is achievable by a plasma-based microlens [30,31] or by deforming a thin foil into a hemisphere [15,32,33] and installing a guiding cone behind the hemisphere [34–36]. Because our focus is on GeV-scale beams, focusing of TNSA ions is further discussed in the Supplemental Material. As the starting point, we develop a model describing the dynamics of a laser-propelled deformable thin target under a simplifying assumption that the target acts as a perfectly reflecting mirror. A similar model in planar 2D geometry has been used in [3], but the full equations of motion were neither presented nor solved.

Deformable mirror model of LILA.—The interaction of a circularly polarized laser wave with a thin dense target, whose thickness $d(r_0)$ decreases from the center toward its edge, can be simplified by modeling the target as an ideal mirror deformed by a slowly changing radiation pressure P applied to the target surface. Because of the variation of the areal mass $dm/dS = m_i n_0 d$ (where m_i is the ion mass and n_0 is the target density), different parts of the target experience different accelerations. The initially flat target bends forward because of the higher velocity of its periphery and is eventually focused to a small area, as shown in Fig. 1. Lagrangian coordinates [37] are adopted with axial symmetry such that $x(r_0, t)$, $r(r_0, t)$ are functions of the time t and the initial radial positions r_0: $x(r_0, t = 0) = 0$ and $r(r_0, t = 0) = r_0$. The number of the δN ions contained in a ring element of width δr_0 and radius r_0 is conserved during its motion: $\delta N = 2\pi n_0 d(r_0) r_0 \delta r_0$. The element's area $\delta S(r_0, t)$ and the unit vector $\vec{n}(r_0, t)$ normal to the element's surface are changing with time according to

$$\delta S = 2\pi r(r_0, t)[r'(r_0, t)^2 + x'(r_0, t)^2]^{1/2} \delta r_0, \quad (1)$$

$$\vec{n} = \frac{r'(r_0, t)\vec{e}_x - x'(r_0, t)\vec{e}_r}{[r'(r_0, t)^2 + x'(r_0, t)^2]^{1/2}}, \quad (2)$$

where $'$ stands for a derivative with respect to r_0, and $(\vec{e}_x, \vec{e}_r)$ are the unit vectors in x and r directions, respectively. When the target moves with the relativistic velocity $\vec{v}$, the photon reflection angle α_r may differ from the incidence angle α_i. However, the change of the photon momentum $\hbar\Delta\vec{k}$ is always directed along the surface normal [38,39]. After application of the momentum conservation, an equation of motion for the target element is obtained:

$$\frac{\delta N}{\delta S}\frac{\partial \vec{p}}{\partial t} = -\kappa\left(\frac{E^2}{2\pi m_i c}\cos\alpha_i\right)\frac{(\beta\cos\phi - \cos\alpha_i)}{(1 - \beta^2\cos^2\phi)}\vec{n}, \quad (3)$$

where $\beta = v/c$ is the dimensionless velocity, E is the laser electric field, $\vec{p} = \vec{\beta}/\sqrt{1-\beta^2}$ is the dimensionless momentum, and $\kappa = (\cos\alpha_i - \beta\cos\phi)/\cos\alpha_i$.

We consider a parabolically shaped target with radius R_0 and thickness given by $d(r_0) = d_0(1 - r_0^2/2R_c^2)$, where d_0 is the target thickness at the center and R_c is the radius of curvature. After normalizing x, r, r_0, ct by R_c and d by d_0, Eq. (3) is transformed to

$$\frac{\partial \vec{p}}{\partial t} = \frac{gR_c}{c^2}\frac{(\cos\alpha_i - \beta\cos\phi)^2}{(1 - \beta^2\cos^2\phi)}\frac{r/r_0}{d(r_0)}(r'\vec{e}_x - x'\vec{e}_r), \quad (4)$$

where $g = E^2/2\pi d_0 m_i n_0$ is the initial acceleration of the central point of the target. The trigonometric functions in Eq. (4) can be expressed as $\cos\phi = \vec{n}\cdot\vec{v}/v$ and $\cos\alpha_i = \vec{n}\cdot\vec{e}_x$. Assuming an initially stationary target [$\vec{p}(r_0, t = 0) = 0$ for all values of $r_0 < R_0/R_c$], we observe that the target dynamics is determined by just two dimensionless parameters: the target radius R_0/R_c and its peak energy $\Gamma \equiv gR_c/c^2$. The final target energy becomes relativistic for $\Gamma \sim 1$.

The results of the numerical solutions of Eq. (4) are presented in Fig. 2, where several time snapshots of the target shape are shown up to the focusing time $t = t_f$. For each laser amplitude [$a_0 = 10$ in (a) and $a_0 = 100$ in (b)], we simulated two initial target radiuses: $R_0 = R_c$ (black lines) and $R_0 = 2R_c/3$ (red line). Overdense $H^+ - e^-$ plasma with $n = 100 n_c$ was used, where $n_c \equiv m_e\omega_0^2/4\pi e^2 = 1.12 \times 10^{21}$ cm^{-3} is the critical density for the laser wavelength $\lambda_0 = 1$ μm. In all four cases, the parabolically shaped target is focused to a very small spot at the focusing distance $x = L_f$, without any aberration. The aberration-free focusing of the parabolic target has been proven analytically under the paraxial approximation; more details can be found in Sec. I of the Supplemental Material [40].

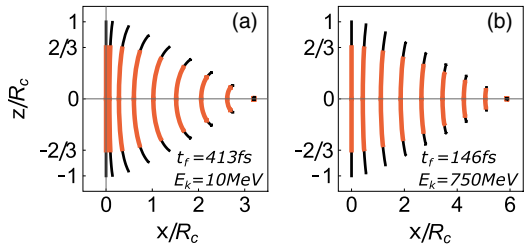

FIG. 2. Deformable mirror model of the acceleration and focusing of a thin target propelled by laser pulses of different normalized amplitudes $a_0 = 10$ ($\Gamma = 0.021$) (a) and $a_0 = 100$ ($\Gamma = 2.1$) (b), and different target radiuses: $R_0 = R_c$ (black curves) and $R_0 = (2/3)R_c$ (red curves). Target parameters: $R_c = 6\ \mu$m, $d_0 = 300$ nm, and $n_0 = 100\ n_c$.

In the subrelativistic case ($\Gamma = 0.021$), the target undergoes significant bending, and its final (per proton) kinetic energy reaches $E_k \approx 10$ MeV at the focal point $L_f \approx 3R_c$. In the relativistic case ($\Gamma = 2.1$), the target bending is smaller, and the final kinetic energy is $E_k \approx 750$ MeV at $L_f \approx 6R_c$. In fact, it can be analytically demonstrated (see Supplemental Material) that $L_f \approx 2.95R_c$ in the subrelativistic limit of $\Gamma \to 0$. In the relativistic ($\Gamma \gg 1$) case, the focusing length L_f monotonically increases with Γ. Another important observation from Fig. 2 is that the focusing length is essentially independent of the initial target radius: both targets with different radiuses focus at the same point. Therefore, within the limits of the deformable mirror (DM) model, the dynamics of the parabolically shaped target is parameterized by Γ alone.

In reality, the applicability of the DM model is limited by the complex dynamics of multispecies plasmas that includes plasma heating (due to the nonplanar nature of the bending target), charge separation, the Coulomb explosion that follows from such separation, and the RT-like instability. Below we demonstrate that, despite the complexity of relativistic laser-plasma interactions, the conclusions of the DM model largely hold, and that simultaneous focusing and acceleration by the LILA mechanism is indeed feasible under a wide range of laser powers.

Particle-in-cell simulations of LILA.—We validate the LILA concept by performing 3D simulations using a PIC code VLPL [41]. In the first example, we assume a fully ionized two-species (electrons and protons) parabolically shaped target with $R_0 = 8\ \mu$m and $R_c = 7\ \mu$m, the initial density $n = 100n_c$, and a circularly polarized planar wave with wavelength $\lambda_0 = 1\ \mu$m and intensity $I = 1.75 \times 10^{22}$ W/cm^2 ($a_0 = 80$). These parameters correspond to the estimated laser power $P = 35$ PW over the target area. The target thickness $d_0 = 300$ nm at its center is chosen to be larger than the optimal thickness [42] $d_{\rm opt} = (\lambda_0/\pi)(n_c/n)a_0 \approx 250$ nm.

As shown in Fig. 3(a), the positions of the target (its bending and focusing) calculated using the code VLPL are

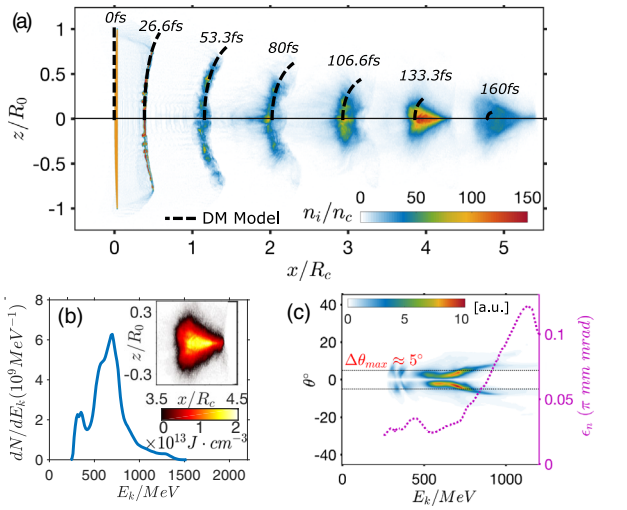

FIG. 3. A 3D PIC simulation of LILA. (a) Snapshots of ion densities. Black-dashed lines: target positions from the DM model. The focal spot (peak plasma density) is achieved at $t_f = 133.3$ fs (b) Proton energy spectrum and energy density distribution (in the inset) at $t = t_f$. (c) Proton phase space (E_k, θ) distribution and normalized emittance ε_n (dotted line) vs energy E_k at $t = t_f$. The laser has a flattop longitudinal profile with a duration $\tau = 45$ fs and a rising edge $\tau_{\rm rise} = 3.3$ fs. The simulation box size is $X \times Y \times Z = 50\lambda_0 \times 20\lambda_0 \times 20\lambda_0$, consists of $5000 \times 250 \times 250$ cells. At the plasma region, each cell contains 160 macroparticles.

very close to those obtained from the DM model. But in contrast to the DM model, the simulation predicts target deterioration at the edges, where its thickness is smaller than $d_{\rm opt}$. Besides, we observe that a realistic plasma target cannot be focused into a point due to its stretching in the x direction. Moreover, only about 50% of the ions are focused into a focal spot measuring less than 4 μm in every dimension. It has been recognized from flat target simulations that a fraction of the ions trails behind the bulk of the target [9,42] and that only some of the ions gain large energy through the RPA mechanism. Nevertheless, despite the target elongation and partial loss of ions, the peak density of the focused ions is ≈1.5 times *larger* than their initial density due to the convergent plasma flow. Another deviation from the DM model is that the focal length $L_f^{(\rm PIC)} \sim 4R_c \approx 28\ \mu$m found from the simulation is slightly shorter than $L_f^{(\rm DM)} \sim 5R_c = 35\ \mu$m predicted by the DM model.

Since in this simulation the value of $\Gamma \approx 1.6$, the target ions at the focal spot are expected to acquire relativistic energies. This is confirmed by the ion energy spectrum peaked at $E_k^{(\rm peak)} \approx 750$ MeV plotted as a solid line in Fig. 3(b). To quantify the degree of directionality of the LILA ions, we have plotted in Fig. 3(c) the normalized emittance $\epsilon_n(E_k)$ [43] as a function of ion energy E_k. Remarkably, $\epsilon_n(E_k)$ has a minimum around $E_k \approx E_{\rm ion}^{(\rm peak)}$,

indicating that the accelerated beam is not only focused and quasimonoenergetic but also highly directional.

Indeed, the proton beam distribution plotted in Fig. 3(c) in the (E_k, θ) phase space (where θ is the angle between ion velocity and the x axis) confirms that the angular spread of the ions at the focal spot is very small: $\Delta\theta_{\max} \approx 5°$. This corresponds to the remarkably low emittance of quasimonoenergetic ions at the focal spot: $\epsilon_{\min} \approx 0.035(\pi \cdot \text{mm} \cdot \text{mrads})$. This low emittance is preserved after the focal point, making the resulting ion beam interesting for a variety of applications that require collimated beams. The high concentration of relativistic ions in such a small focal volume results in an extremely high energy density u_k plotted in the inset of Fig. 3(b), with its peak reaching $u_k^{\max} \approx 2 \times 10^{13}$ J $\cdot$ cm^{-3}. Note that only the $\tau_L \approx 46.6$ fs pulse length is needed until the focal point is reached. The laser energy U_L contained within the volume $V_L = c\tau_L \times \pi R_0^2$ is $U_L \approx 1.6$ kJ; a considerable fraction $\eta \approx 16\%$ of U_L is transferred to the ions at the hot focal spot.

LILA scaling and stability.—With the DM model validated by 3D PIC simulation for at least some laser and target parameters, we next obtain simple scalings of the target's energy and focal distance that apply for a wide parameter range. As demonstrated earlier, the dynamics of the target focusing and acceleration within the DM model is determined by a single dimensionless parameter Γ. In particular (see Supplemental Material), the ion momentum p_x at the focal point and the focusing length L_f in this model can be approximated by the following expressions:

$$p_x/m_i c \approx \Gamma^{1/2}, \qquad L_f/R_c \approx 2\Gamma^{1/2} + 2.95. \tag{5}$$

Approaching these scalings requires that the target does not succumb to RT-like instability. Therefore, a series of simulations are carried out to examine the influence of the RT-like instability on the target focusing and to verify the scalings given by Eq. (5). The results of these simulations corresponding to the dimensionless Γ and R_c/λ_0 listed in Table I are shown in Fig. 4. Three simulations with different values of R_c/λ_0 are performed for each value of Γ and the following target parameters are used: radius $R_0 = 1.14R_c$, maximum thickness $d_0 = 1.2d_{\text{opt}}$, and density $n_0 = 100\, n_c$ (see Supplemental Material for the reasons these parameters were chosen).

Stable LILA regimes are identified by analyzing the size of the hot spot as well as the particle and energy densities

TABLE I. Simulation parameters.

	$\Gamma^{1/2}$(PW)[a]	0.67(2.8)	0.87(8)	1.07(18)	1.27(35)
x	R_c/λ_0	1.9	2.6	3.4	4.1
•	R_c/λ_0	3.2	4.5	5.8	7.0
▲	R_c/λ_0	6.2	7.5	8.8	10

[a]Laser power in petawatts.

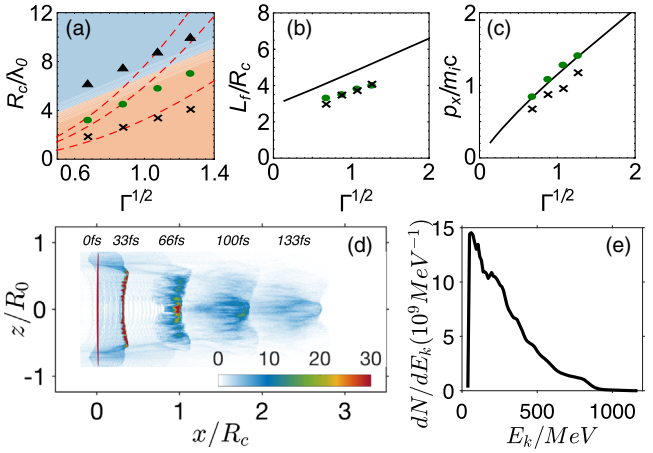

FIG. 4. Parameter scan of LILA target in 3D PIC simulations. (a) Stable (crosses, bullets) and unstable (triangles) target focusing in the (Γ, R_c) parameter space. Red dashed lines represent constant acceleration contours (from top to bottom): $g = 0.13c^2/\lambda_0$, $0.17c^2/\lambda_0$, and $0.30c^2/\lambda_0$. (b) Focal length L_f and (c) momentum p_x as functions of $\sqrt{\Gamma}$ from the DM model (solid line) and 3D PIC simulations (crosses, bullets). (d) Example of the unstable acceleration and focusing of the target, corresponds to $\Gamma = 1.6$ and $R_c/\lambda_0 = 10$. (e) Ions' energy spectrum of the unstable target in (d) at moment $t = 133$ fs.

within it. For example, the simulation results shown in Fig. 3 corresponding to $\Gamma = 1.6$ and $R_c/\lambda_0 = 7$ exemplify a stable focusing case. Strong convergence of the target appears to suppress the instability. In fact, one of the characteristic signatures of the RT-like instability is the breakup of the target into multiple clumps. Such an instability onset is indeed observed at $t \approx 26.6$ fs. However, the clumps converge toward the axis and merge at later times, thereby effectively suppressing the instability. On the contrary, Fig. 4(d) shows a typical example of *unstable* target focusing corresponding to $\Gamma = 1.61$ and $R_c/\lambda_0 = 10$. The RT-like instability breaks the target into large density clumps, the RPA fails to focus the target, and the acceleration terminates because the entire target becomes transparent to the laser after $t = 66$ fs. When compared to the focused target in Fig. 3, the peak ion density of the RT-unstable target is reduced by 1 order of magnitude, and the ion energy spectrum shown in Fig. 4(e) is no longer monoenergetic.

One immediate observation from Figure 4(a) is that, for a given laser power, the target focusing is stabilized at small values of R_c but is disrupted for larger targets. Qualitatively, this can be understood by observing that a larger R_c corresponds to a longer focusing time, thus supporting more e-foldings for developing RT-like instability. Figure 4(a) further implies that, although higher acceleration may slow down the development of instability due to the relativistic effect [3,5], that is not the main reason why the instabilities are suppressed: the two targets on the second red dashed line have the same acceleration:

$g = 0.17c^2/\lambda_0$, but the target with the bigger R_c [shown in Fig. 4(d)] still breaks at the early stage. The same thing happened for the two targets sitting on the $g = 0.13c^2/\lambda$ line. Not surprisingly, whenever the conditions for stable acceleration and focusing are met, the predictions of the DM model for the focal length L_f and the ion momentum p_x are very accurate. Indeed, the results obtained with simulations are in agreement with Eq. (5), as shown in Fig. 4(b),(c).

Discussion and outlook.—Simultaneous acceleration and focusing of the variable-thickness LILA targets have been shown to be stable under various laser powers, ranging from 2.8 to 35 PW. Near the lower end of this power range, ultrashort circularly polarized lasers are already available [44,45]. The 10s-PW lasers will soon become accessible at several user facilities worldwide [46–48]. The LILA targets are also robust under various laser-target configurations. Realistic LILA targets composed of proton-rich materials (e.g., F8DT polymers [45]) should behave similarly to pure hydrogen targets as long as the dimensionless Γ is rescaled to account for the effective Z/M ratio of a multispecies target. This conclusion is also confirmed by a 3D-PIC simulation (see the Supplemental Material, which includes Refs. [49,50]) of a C-H LILA target.

Furthermore, LILA targets can be successfully focused by realistic laser pulses with nonplanar transverse profiles. This is accomplished by correcting the target thickness profile $d(r_0)$ according to the transverse profile of the pulse. For a Gaussian laser pulse [$I = I_0 \exp(-r^2/\sigma_L^2)$], the DM model predicts that the target thickness profile can be corrected according to $d(r_0) \to d(r_0)\exp(-r^2/\sigma_L^2)$. Our 3D-PIC simulations (see Supplemental Material) support this conclusion. For a flat target, we observe considerable broadening of the energy spectrum, as well as severe increases in the angular spread and emittance of the proton beam when compared to a LILA target of the same size, density, and average thickness (see Fig. S5 in the Supplemental Material). Advances in laser and nanofabrication technologies will enable the experimental realization of our theoretical concept. Current laser technology is steadily progressing toward high-contrast PW laser pulses with contrasts well above 10^{12} [51,52], thereby avoiding deleterious preplasma generation. The scaling laws presented here enable designing the target geometry and selecting the appropriate laser power and duration. Depending on those parameters, a wide range of ion kinetic energies—from 200 to 750 MeV—can be obtained with many future applications in sight. These include ion accelerators for cancer treatment [53] and novel spallation sources [20].

This work is supported by the award from the HEDLP NNSA Grant No. NA0003879. The authors thank the Texas Advanced Computing Center (TACC) at The University of Texas at Austin for providing HPC resources.

[1] T. Esirkepov, M. Borghesi, S. V. Bulanov, G. Mourou, and T. Tajima, Highly Efficient Relativistic-Ion Generation in the Laser-Piston Regime, Phys. Rev. Lett. **92**, 175003 (2004).

[2] A. Macchi, F. Cattani, T. V. Liseykina, and F. Cornolti, Laser Acceleration of Ion Bunches at the Front Surface of Overdense Plasmas, Phys. Rev. Lett. **94**, 165003 (2005).

[3] F. Pegoraro and S. V. Bulanov, Photon Bubbles and Ion Acceleration in a Plasma Dominated by the Radiation Pressure of an Electromagnetic Pulse, Phys. Rev. Lett. **99**, 065002 (2007).

[4] A. Robinson, M. Zepf, S. Kar, R. Evans, and C. Bellei, Radiation pressure acceleration of thin foils with circularly polarized laser pulses, New J. Phys. **10**, 013021 (2008).

[5] B. Qiao, M. Zepf, M. Borghesi, and M. Geissler, Stable GeV Ion-Beam Acceleration from Thin Foils by Circularly Polarized Laser Pulses, Phys. Rev. Lett. **102**, 145002 (2009).

[6] E. Fourkal, I. Velchev, and C.-M. Ma, Coulomb explosion effect and the maximum energy of protons accelerated by high-power lasers, Phys. Rev. E **71**, 036412 (2005).

[7] E. Ott, Nonlinear Evolution of the Rayleigh-Taylor Instability of a Thin Layer, Phys. Rev. Lett. **29**, 1429 (1972).

[8] C. A. J. Palmer *et al.*, Rayleigh-Taylor Instability of an Ultrathin Foil Accelerated by the Radiation Pressure of an Intense Laser, Phys. Rev. Lett. **108**, 225002 (2012).

[9] V. Khudik, S. Yi, C. Siemon, and G. Shvets, The analytic model of a laser-accelerated plasma target and its stability, Phys. Plasmas **21**, 013110 (2014).

[10] F. Brunel, Not-so-Resonant, Resonant Absorption, Phys. Rev. Lett. **59**, 52 (1987).

[11] F. Brunel, Anomalous absorption of high intensity subpicosecond laser pulses, Phys. Fluids **31**, 2714 (1988).

[12] F. Dollar, C. Zulick, A. G. R. Thomas, V. Chvykov, J. Davis, G. Kalinchenko, T. Matsuoka, C. McGuffey, G. M. Petrov, L. Willingale, V. Yanovsky, A. Maksimchuk, and K. Krushelnick, Finite Spot Effects on Radiation Pressure Acceleration from Intense High-Contrast Laser Interactions with Thin Targets, Phys. Rev. Lett. **108**, 175005 (2012).

[13] M. Tabak, J. Hammer, M. E. Glinsky, W. L. Kruer, S. C. Wilks, J. Woodworth, E. M. Campbell, M. D. Perry, and R. J. Mason, Ignition and high gain with ultrapowerful lasers, Phys. Plasmas **1**, 1626 (1994).

[14] S. Atzeni, M. Temporal, and J. Honrubia, A first analysis of fast ignition of precompressed ICF fuel by laser-accelerated protons, Nucl. Fusion **42**, L1 (2002).

[15] P. Patel, A. Mackinnon, M. Key, T. Cowan, M. Foord, M. Allen, D. Price, H. Ruhl, P. Springer, and R. Stephens, Isochoric Heating of Solid-Density Matter with an Ultrafast Proton Beam, Phys. Rev. Lett. **91**, 125004 (2003).

[16] G.. M. Dyer, A. C. Bernstein, B. I. Cho, J. Osterholz, W. Grigsby, A. Dalton, R. Shepherd, Y. Ping, H. Chen, K. Widmann, and T. Ditmire, Equation-of-State Measurement of Dense Plasmas Heated With Fast Protons, Phys. Rev. Lett. **101**, 015002 (2008).

[17] S. Bulanov, T. Z. Esirkepov, V. Khoroshkov, A. Kuznetsov, and F. Pegoraro, Oncological hadrontherapy with laser ion accelerators, Phys. Lett. A **299**, 240 (2002).

[18] A. Yogo *et al.*, Application of laser-accelerated protons to the demonstration of DNA double-strand breaks in human cancer cells, Appl. Phys. Lett. **94**, 181502 (2009).
[19] P. Bolton, T. Hori, H. Kiriyama, M. Mori, H. Sakaki, K. Sutherland, M. Suzuki, J. Wu, and A. Yogo, Toward integrated laser-driven ion accelerator systems at the photo-medical research center in Japan, Nucl. Instrum. Methods Phys. Res., Sect. A **620**, 71 (2010).
[20] P. McKenna, K. W. D. Ledingham, S. Shimizu, J. M. Yang, L. Robson, T. McCanny, J. Galy, J. Magill, R. J. Clarke, D. Neely, P. A. Norreys, R. P. Singhal, K. Krushelnick, and M. S. Wei, Broad Energy Spectrum of Laser-Accelerated Protons for Spallation-Related Physics, Phys. Rev. Lett. **94**, 084801 (2005).
[21] F. Hannachi, M. Alonard, M. Gerbaux, F. Gobet, G. Malka, C. Plaisir, J. Scheurer, M. Tarisien, P. Audebert, E. Brambrink, V. Mot, P. Morel, Ph. Nicola, and V. Tikhonchuk, Prospects for nuclear physics with lasers, Plasma Phys. Controlled Fusion **49**, B79 (2007).
[22] M. Perry, D. Pennington, B. Stuart, G. Tietbohl, J. Britten, C. Brown, S. Herman, B. Golick, M. Kartz, J. Miller, H. T. Powell, M. Vergino, and V. Yanovsky, Petawatt laser pulses, Opt. Lett. **24**, 160 (1999).
[23] S. V. Bulanov, E. Y. Echkina, T. Z. Esirkepov, I. N. Inovenkov, M. Kando, F. Pegoraro, and G. Korn, Unlimited Ion Acceleration by Radiation Pressure, Phys. Rev. Lett. **104**, 135003 (2010).
[24] X. Q. Yan, C. Lin, Z.-M. Sheng, Z. Y. Guo, B. C. Liu, Y. R. Lu, J. X. Fang, and J. E. Chen, Generating High-Current Monoenergetic Proton Beams by a Circularly Polarized Laser Pulse in the Phase-StableAcceleration Regime, Phys. Rev. Lett. **100**, 135003 (2008).
[25] R. A. Snavely *et al.*, Intense High-Energy Proton Beams from Petawatt-Laser Irradiation of Solids, Phys. Rev. Lett. **85**, 2945 (2000).
[26] S. P. Hatchett *et al.*, Electron, photon, and ion beams from the relativistic interaction of petawatt laser pulses with solid targets, Phys. Plasmas **7**, 2076 (2000).
[27] L. O. Silva, M. Marti, J. R. Davies, R. A. Fonseca, C. Ren, F. S. Tsung, and W. B. Mori, Proton Shock Acceleration in Laser-Plasma Interactions, Phys. Rev. Lett. **92**, 015002 (2004).
[28] L. Ji, B. Shen, X. Zhang, F. Wang, Z. Jin, X. Li, M. Wen, and J. R. Cary, Generating Monoenergetic Heavy-Ion Bunches with Laser-Induced Electrostatic Shocks, Phys. Rev. Lett. **101**, 164802 (2008).
[29] L. Yin, B. Albright, B. Hegelich, and J. Fernndez, GeV laser ion acceleration from ultrathin targets: The laser break-out afterburner, Laser Part. Beams **24**, 291 (2006).
[30] T. Toncian, M. Borghesi, J. Fuchs, E. d'Humieres, P. Antici, P. Audebert, E. Brambrink, C. A. Cecchetti, A. Pipahl, L. Romagnani, and O. Willi, Ultrafast laser-driven microlens to focus and energy-select mega-electron volt protons, Science **312**, 410 (2006).
[31] T. Toncian, M. Amin, M. Borghesi, C. A. Cecchetti, R. J. Clarke, J. Fuchs, R. Jung, T. Kudyakov, M. Notley, A. C. Pipahl, P. A. Wilson, and O. Willi, Properties of a plasma-based laser-triggered micro-lens, AIP Adv. **1**, 022142 (2011).
[32] R. A. Snavely *et al.*, Laser generated proton beam focusing and high temperature isochoric heating of solid matter, Phys. Plasmas **14**, 092703 (2007).
[33] D. T. Offermann, K. A. Flippo, J. Cobble, M. J. Schmitt, S. A. Gaillard, T. Bartal, D. V. Rose, D. R. Welch, M. Geissel, and M. Schollmeier, Characterization and focusing of light ion beams generated by ultra-intensely irradiated thin foils at the kilojoule scale, Phys. Plasmas **18**, 056713 (2011).
[34] T. Bartal *et al.*, Focusing of short-pulse high-intensity laser-accelerated proton beams, Nat. Phys. **8**, 139 (2012).
[35] B. Qiao, M. E. Foord, M. S. Wei, R. B. Stephens, M. H. Key, H. McLean, P. K. Patel, and F. N. Beg, Dynamics of high-energy proton beam acceleration and focusing from hemisphere-cone targets by high-intensity lasers, Phys. Rev. E **87**, 013108 (2013).
[36] C. McGuffey, J. Kim, M. S. Wei, P. M. Nilson, S. N. Chen, J. Fuchs, P. Fitzsimmons, M. E. Foord, D. Mariscal, H. S. McLean, P. K. Patel, R. B. Stephens, and F. N. Beg, Focussing protons from a kilojoule laser for intense beam heating using proximal target structures, Sci. Rep. **10**, 9415 (2020).
[37] B. R. Munson, T. H. Okiishi, A. P. Rothmayer, and W. W. Huebsch, *Fundamentals of Fluid Mechanics* (John Wiley & Sons, New York, 2014).
[38] A. Gjurchinovski, Reflection of light from a uniformly moving mirror, Am. J. Phys. **72**, 1316 (2004).
[39] J. R. Galli and F. Amiri, A general principle for light reflecting from a uniformly moving mirror: A relativistic treatment, Am. J. Phys. **80**, 680 (2012).
[40] See Supplemental Material at http://link.aps.org/supplemental/10.1103/PhysRevLett.126.024801 for we show the analytical description of the LILA target, details of the electron density evolution, charge neutrality in the focusing process, and more 3D simulation examples with different target configurations and laser profiles.
[41] A. Pukhov, Three-dimensional electromagnetic relativistic particle-in-cell code VLPL (Virtual Laser Plasma Lab), J. Plasma Phys. **61**, 425 (1999).
[42] V. Tripathi, C.-S. Liu, X. Shao, B. Eliasson, and R. Z. Sagdeev, Laser acceleration of monoenergetic protons in a self-organized double layer from thin foil, Plasma Phys. Controlled Fusion **51**, 024014 (2009).
[43] T. E. Cowan *et al.*, Ultralow Emittance, Multi-MeV Proton Beams from a Laser Virtual-Cathode Plasma Accelerator, Phys. Rev. Lett. **92**, 204801 (2004).
[44] J. H. Sung, H. W. Lee, J. Y. Yoo, J. W. Yoon, C. W. Lee, J. M. Yang, Y. J. Son, Y. H. Jang, S. K. Lee, and C. H. Nam, 4.2 PW, 20 fs Ti: sapphire laser at 0.1 Hz, Opt. Lett. **42**, 11 (2017).
[45] I. J. Kim, K. H. Pae, I. W. Choi, CL. Lee, H. T. Kim, H. Singhal, J. H. Sung, S. K. Lee, H. W. Lee, P. V. Nickles, T. M. Jeong, C. M. Kim, and C. H. Nam, Radiation ressure acceleration of protons to 93 MeV with circularly polarized petawatt laser pulses, Phys. Plasmas **23**, 7 (2016).
[46] G. A. Mourou, G. Korn, W. Sandner, and J. L. Collier, *ELI-Extreme Light Infrastructure Science and Technology with Ultra-Intense Lasers Whitebook* (THOSS Media GmbH, Berlin, 2011).
[47] B. Le Garrec, D. N. Papadopoulos, C. Le Blanc, J. P. Zou, G. Chriaux, P. Georges, F. Druon, L. Martin, L. Frneaux, A. Beluze, N. Lebas, F. Mathieu, and P. Audebert, Design update and recent results of the Apollon 10 PW facility, Proc. SPIE Int. Soc. Opt. Eng. **10238**, 80 (2017).

[48] W. Li *et al.*, 339 J high-energy Ti: Sapphire chirped-pulse amplifier for 10 PW laser facility, Opt. Lett. **43**, 22 (2018).
[49] T. P. Yu, A. Pukhov, G. Shvets, and M. Chen, Stable Laser-Driven Proton Beam Acceleration from a Two-Ion-Species Ultrathin Foil, Phys. Rev. Lett. **105**, 065002 (2010).
[50] T. P. Yu, A. Pukhov, G. Shvets, M. Chen, T. H. Ratliff, S. A. Yi, and V. Khudik, Simulations of stable compact proton beam acceleration from a two-ion-species ultrathin foil, Phys. Plasmas **18**, 043110 (2011).
[51] J. M. Mikhailova, A. Buck, A. Borot, K. Schmid, C. Sears, G. D. Tsakiris, F. Krausz, and L. Veisz, Ultra-high-contrast few-cycle pulses for multipetawatt-class laser technology, Opt. Lett. **36**, 3145 (2011).
[52] Y. Wang, S. Wang, A. Rockwood, B. M. Luther, R. Hollinger, A. Curtis, C. Calvi, C. S. Menoni, and J. J. Rocca, 0.85 PW laser operation at 3.3 Hz and high-contrast ultrahigh-intensity $\lambda = 400$ nm second-harmonic beamline, Opt. Lett. **42**, 19 (2017).
[53] D. Schardt, T. Elsasser, and D. Schulz-Ertner, Heavy-ion tumor therapy: Physical and radiobiological benefits, Rev. Mod. Phys. **82**, 383 (2010).